Optical frequency generation using fiber Bragg grating filters for applications in portable quantum sensing

Macrae, Calum D; Bongs, Kai; Holynski, Michael

DOI:
10.1364/OL.415963

Document Version
Publisher's PDF, also known as Version of record

Citation for published version (Harvard):
Macrae, CD, Bongs, K & Holynski, M 2021, 'Optical frequency generation using fiber Bragg grating filters for applications in portable quantum sensing', *Optics Letters*, vol. 46, no. 6, pp. 1257-1260. https://doi.org/10.1364/OL.415963

Optics Letters

Optical frequency generation using fiber Bragg grating filters for applications in portable quantum sensing

Calum D. Macrae,* Kai Bongs, and Michael Holynski

University of Birmingham, School of Physics and Astronomy, Edgbaston, Birmingham, B15 2TT, UK
**Corresponding author: calumdonaldmacrae@gmail.com*

Received 1 December 2020; revised 13 January 2021; accepted 14 January 2021; posted 14 January 2021 (Doc. ID 415963); published 4 March 2021

A method for the agile generation of the optical frequencies required for laser cooling and atom interferometry of rubidium is demonstrated. It relies on fiber Bragg grating technology to filter the output of an electro-optic modulator and was demonstrated in an alignment-free, single-seed, frequency-doubled fiber laser system. The system was capable of frequency switching over a 30 GHz range in less than 40 ns, with ∼0.5 W output power and amplitude modulation with a ∼15 ns rise/fall time and an extinction ratio exceeding 80 dB. The technology is ideal for enabling high-bandwidth, mobile industrial, and space applications of quantum technologies.

https://doi.org/10.1364/OL.415963

Since its inception in 1991 [1], atom interferometry has been used to measure rotation [2], gravitational acceleration [3], gravity gradients [4], and to test the equivalence principle [5]. Given sensing based on atom interferometry has demonstrated exceptionally low instrument drift and suppression of vibrational noise [6], there is particular interest in developing portable quantum devices. These could enable future applications of atom interferometry in civil engineering [7] and space-based sensors [8].

Generally, atom interferometry, as well as laser cooling techniques, impose stringent requirements on the laser system. For example, multiple optical frequencies must be generated with mrad phase coherence over the single shot measurement time; optical frequency sweeping is required during laser cooling and to compensate Doppler-shift during the free fall of atoms [9]; a high amplitude extinction ratio is required to maintain atomic coherence during pulse sequences; and fast optical frequency switching is required to maximize the measurement bandwidth. Furthermore, for portable sensing applications, compactness and robustness is required. For rubidium atom interferometry, these requirements can be met by using a single-seed, frequency-doubled, telecom fiber laser system.

Several single-seed laser systems, which aim to minimize size and power consumption, have been published for rubidium atom interferometry. In 2015 [10], by modulating a 1560 nm seed laser, optical single-sideband modulation over a ∼1 GHz range in a few ms was achieved. In 2016 [11], an approach was taken where a 1560 nm seed laser was locked to an atomic reference, and a Fabry–Perot cavity was used to filter the carrier and undesired sidebands from the output. This allowed optical single-sideband modulation over a ∼1 GHz range in less than 200 μs. However, only a factor of 5 suppression of the undesired sidebands was achieved. Finally, in 2018 [12], a direct 780 nm diode laser approach was used. Although capable of a 578 MHz frequency modulation in 10 ms, the use of tapered amplifiers caused problems in optical power and mode stability. Serrodyne frequency shifting has also been demonstrated as an alternative wideband, single-sideband modulation technique [13]. However, this requires radio-frequency (RF) sawtooth waveform generation, which is difficult to implement at high frequencies, resulting in a relatively low suppression of the optical carrier frequency.

When generating multiple optical frequencies, previous single-seed systems used an electro-optic modulator (EOM) to generate optical double-sideband spectra. This serves to decrease the efficiency of optical amplification as power is wasted in the undesired sidebands. This also affects the systems accuracy by introducing additional interactions [14]. Optical in-phase and quadrature (IQ) modulation has been demonstrated to avoid such effects [15], but requires relatively complex RF signal generation and drift of the modulator's bias points must be compensated [16].

In this paper, by utilizing fiber Bragg grating (FBG) technology, a laser system that can optical single-sideband modulate over a 30 GHz range with frequency jumps in less than 40 ns is presented. Unlike previous systems, multiple frequencies can be generated with a high suppression of all undesired optical frequencies (see Supplement 1). Furthermore, due to the non-linear efficiency of sum frequency generation [17], fast amplitude modulation with a remarkably high extinction ratio can be achieved at 780 nm by modulating at 1560 nm before frequency conversion. This enables the generation of high power, fast pulse sequences with a very high extinction ratio.

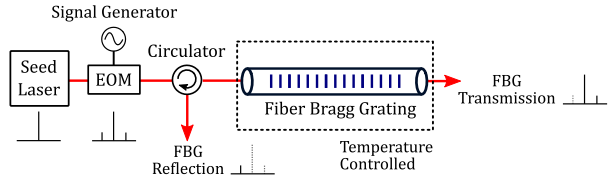

Fig. 1. Optical filtering of the output of an electro-optic modulator (EOM) using a fiber Bragg grating (FBG). The light reflected from the FBG is separated using an optical circulator. The optical spectrum is depicted at various points in the setup.

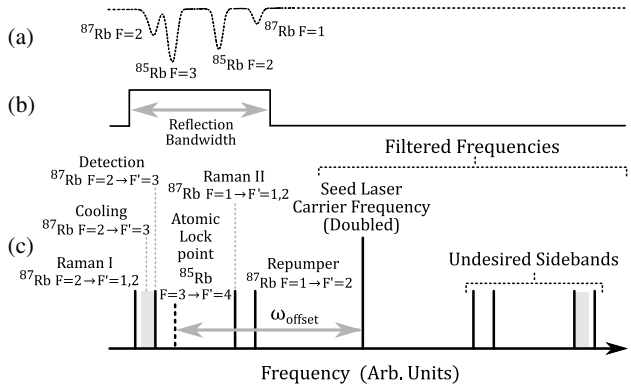

Fig. 2. Fiber Bragg grating is tuned to reflect only the frequencies required for laser cooling and atom interferometry, and to transmit the carrier and undesired sidebands. (a) The absorption spectrum of the rubidium D_2 line, (b) the ideal reflection response of the fiber Bragg grating, and (c) the frequencies required for laser cooling and atom interferometry.

An FBG is a single mode optical fiber with a periodic modulation of the core refractive index, causing light at the Bragg wavelength to be reflected [18]. Since the effective refractive index is dependent on the fiber core temperature and strain [18], commercial FBG filters are sold in thermally controlled enclosures that stabilize strain and allow thermal tuning of the Bragg wavelength over a ∼60 GHz range [19], while remaining stable to <1 GHz. They are available with a 50 MHz to 50 GHz reflection bandwidth [19], which like the center Bragg wavelength, is fixed at manufacture. The reflection frequency response is sufficiently sharp to remove sidebands ≥10 GHz from the output of an EOM with >20 dB attenuation of the carrier and undesired sidebands at 1560 nm. This is achieved by filtering the output of an EOM using an FBG, as shown in Fig. 1. Notably, multiple FBGs can be used to further increase the attenuation of undesired frequencies.

By offset-locking a seed laser to an atomic transition and tuning an FBG to reflect one set of sidebands from an EOM, single-sideband spectra can be generated over the entire range required for laser cooling and atom interferometry (Fig. 2). This enables agile single-sideband modulation limited only by the electro-optic modulation bandwidth, which can exceed 30 GHz in fiber-coupled EOMs [20]. Figure 3 shows an implementation of the optical filtering scheme in a single-seed laser system.

The transmission from the first FBG (TFN-1560.746-N50-IL3.5-30-C1P-C3, TeraXion) was used to offset-frequency-lock the seed laser (Koheras Basik E15, NKT) to the $F = 3$ to $F' = 4$ transition of the ^{85}Rb D_2 line (Ω_{lock}) using modulation transfer spectroscopy (MTS) [21]. MTS was used as it is robust to

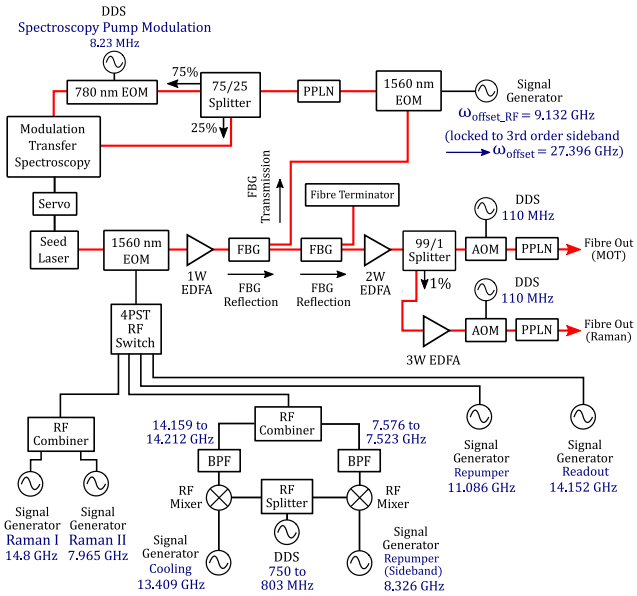

Fig. 3. Simplified diagram of the laser system used to laser cool and measure two-photon Raman transitions in rubidium atom ensembles. The output optical frequency was switched using the quadruple-pole-single-throw (4PST) radio-frequency (RF) switch connected to the electro-optic modulator (EOM). The RF input was filtered with bandpass filters (BPFs), and frequency sweeps were implemented with direct-digital synthesizers (DDSs). The transmission from the first fiber Bragg grating (FBG) was used to offset-lock the seed laser to an atomic reference. The reflection was passed through a second FBG to further attenuate the undesired optical frequencies, then amplified with erbium-doped fiber amplifiers (EDFAs), amplitude modulated with acousto-optic modulators (AOMs), and frequency converted with periodically poled lithium niobate (PPLN) waveguides.

laser amplitude fluctuations, and the laser lock signal is only affected by the resonant EOM sideband and not by the carrier or sidebands that do not fulfil the modulation transfer resonance condition [21]. A fiber-coupled MTS setup was built, and a servo controller (LB1005-S, Newport) maintained the lock. The atomic offset frequency (ω_{offset}) was ∼27.3 GHz, achieved by locking to the EOM's third-order sideband using a frequency of ∼9.1 GHz and an RF power of 19.1 dBm. Switching between cooling, state preparation, Raman, and readout frequencies was achieved using an RF switch (EVAL-ADRF5044, Analog Devices). The switching time was measured with a 4 GHz oscilloscope (DSO9404A, Agilent) by converting the RF switch output to a DC signal with an RF mixer (ZX05-153LH-S+, Mini Circuits). EOMs were used to phase modulate at 1560 nm (MPZ-LN-10, iXblue) for frequency generation and at 780 nm (NIR-MPX800, iXblue) in the MTS setup. The laser system's optical single-sideband modulation range was tested using a wavelength meter (WS-U, HighFinesse), and optical spectra were measured using a scanning Fabry–Perot interferometer (SA200-5B, Thorlabs). Optical amplitude modulation was achieved using acousto-optic modulators (AOMs) (T-M110-0.2C2J-3-F2P, Gooch and Housego), and a biased InGaAs detector (DET10N2, Thorlabs) and 4 GHz oscilloscope (DSO9404A, Agilent) were used to characterize the rise/fall times. The extinction ratio was measured using an optical powermeter (S132C, Thorlabs).

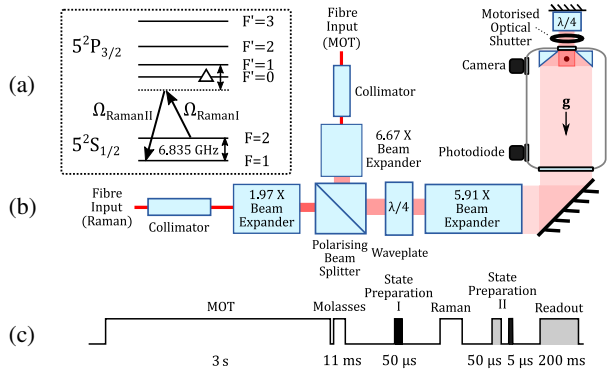

Fig. 4. (a) Raman transition energy level diagram where Δ is the Raman detuning; (b) configuration of vacuum chamber, sensors, free-space optics, and the direction of gravitational acceleration **g**; and (c) experimental pulse sequence (not to scale). Black and gray pulses are resonant with F = 1 to F′ = 2 and F = 2 to F′ = 3 transitions of the ^{87}Rb D_2 line, respectively.

A temperature-controlled, fiber-coupled periodically poled lithium niobate waveguide (WH-0780-000-F-BC, NTT Electronics) was used to convert from 1560 to 780 nm. A 1 W erbium-doped fiber amplifier (EDFA) (ML1-EYFA-CW-SLM-P-OEM-SOA-1560, NKT), 2 W EDFA (F-CEFA-759-00, NKT), and 3 W EDFA (YEDFA-PM-EM-3W-FC/APC-FC/APC-0, Orion Laser) were used to amplify the light to 500 mW and 2 W before the first FBG and the AOMs, respectively. Maximal optical power was input to the FBG to allow minimal RF power (∼ − 7 dBm) to be applied to the EOM, thus minimizing the amplitude of the EOM harmonics. These were not filtered by the FBG as the FBG reflection bandwidth (50 GHz) was too high and the EOM frequency range used (7 to 15 GHz) was too low. Although the insertion loss per FBG is nominally <3.5 dB [19], at these RF powers, only 50 µW optical power reached the 2 W EDFA. RF synthesizer evaluation boards (LMX2594EVM and LMX2595EVM, Texas Instruments), direct-digital synthesizer evaluation boards (EVAL-AD9914, Analog Devices), an arbitrary waveform generator (SDG6022X, Siglent), and a signal generator (E82667D, Keysight) were used to generate the required RF frequencies. The evaluation boards were programmed using microprocessors (PIC18F47K42 and PIC18F27K42, Microchip) and triggering was achieved using a CompactRIO Single-Board Controller (sbRio 9627, National Instruments). The laser system was connected to the free-space section [Fig. 4(b)] via optical fibers. Here, the light was collimated and expanded, and a quarter-wave plate was used for conversion from linear to circular polarization. The light was coupled into a vacuum chamber, and a magneto-optical trap (MOT) beam geometry was formed using light reflected from four prisms and a mirror. A quarter-wave plate inserted before the mirror ensured retro-reflected beams maintained the same circular polarization handedness and a motorized optical shutter (SHB1T, Thorlabs) enabled blocking of the mirror and quarter-wave plate during Raman and readout pulses. Magnetic fields were generated by passing current through wire coils surrounding the chamber. Atomic fluorescence was measured with an unbiased photodiode (SM05PD1A, Thorlabs), and data were recorded with an oscilloscope (4262, Pico Technology).

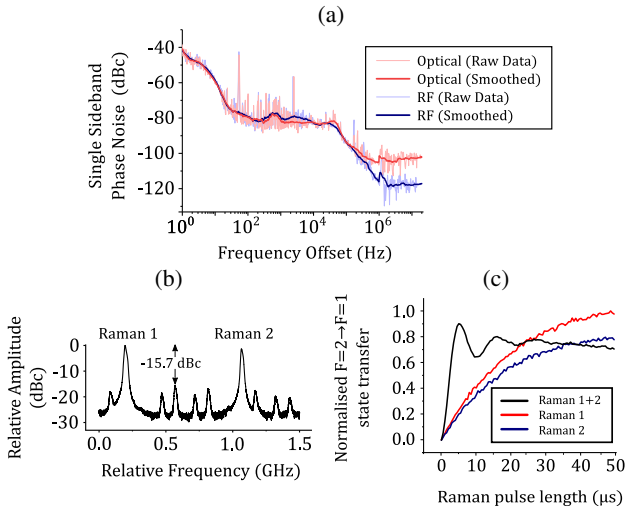

Fig. 5. (a) Measurement of single-sideband phase noise of the optical and RF beat notes at 6.835 GHz. (b) Measurement of the laser optical spectrum during Raman pulses. The data were averaged four times. (c) Rabi oscillations of copropagating two-photon Raman transition obtained by varying the Raman pulse length. A Raman detuning of Δ = 850 MHz was used, and the data were averaged four times.

To compare the phase noise of the laser output with the RF used to generate it, a fast photodiode (125G-010HR-FC, Osi Optoelectronics) was used to measure the 6.835 GHz beat frequency during Raman pulse output. The same frequency was generated with an RF mixer (ZX05-24MH-S+, Mini Circuits) using the frequencies input to the EOM. The phase noise of both signals was measured using a spectrum analyzer (N9030B, Keysight).

The laser system was verified to optical single-sideband modulate over a 30 GHz range using RF frequencies from 5 to 20 GHz. It was capable of generating Raman and MOT beams with approximate beam diameters of 17 and 58 mm and powers of 341 and 539 mW, respectively. The amplitude modulation rise and fall times were measured to be 14.2 ± 0.3 ns and 16.4 ± 0.2 ns, respectively. The amplitude extinction ratio of the laser system exceeded the 80 dB dynamic range of the powermeter (S132C, Thorlabs). At 1560 nm, the AOM extinction ratio was measured to be 60 ± 1 dB, and due to the quadratic power dependency of frequency conversion [17], the extinction ratio is calculated to be 120 ± 2 dB at 780 nm. The RF switching time, which limits the optical switching time, was measured to be below 40 ns.

Figure 5(a) shows the single-sideband phase noise of the optical and RF beat notes when outputting Raman pulses. The phase noise of the optical signal closely follows the RF source up to a ∼20 kHz offset without the use of phase-locking electronics, demonstrating successful RF to optical conversion.

Figure 5(b) shows the optical spectrum of the laser when outputting Raman pulses. Because the Fabry–Perot interferometer had a nominal free-spectral range of 1.5 GHz, the two Raman frequencies are observed as peaks spaced ∼835 MHz apart. Multiple spurious frequencies were also observed due to the undesired component of sum frequency generation (see Supplement 1) as well as sum frequency generation of the undesired carrier frequency, EOM sidebands, and harmonics. Overall, undesired optical frequencies were suppressed by ∼15.7 dB at 780 nm. However, at the time of measurement,

one of the FBGs had one of four thermoelectric coolers nonfunctional, likely reducing its performance. Suppression was ∼4.3 dB below that achieved by IQ modulation [15]; however, unlike with IQ modulators, performance could be improved by adding additional FBGs. This is the first single-seed laser system providing both cooling and Raman light that avoids generating the Raman frequencies using a double-sideband method. Therefore, the suppression of undesired frequencies during Raman pulse sequences is improved by >12 dB compared with previous single-seed systems [10–12].

Figure 5(c) shows Rabi oscillations of a copropagating two-photon Raman transition in ensembles of cold rubidium atoms obtained by varying the Raman pulse length. A Raman detuning (Δ) of 850 MHz relative to the $F' = 1$ state [Fig. 4(a)] was used, and the experimental pulse sequence is shown in Fig. 4(c). The atomic cloud was dropped ∼15 cm before readout, and the Raman pulses occurred during free fall. Figure 5(c) shows that only when both Raman I and Raman II optical frequencies are applied, are oscillations observed. This demonstrates the successful cooling, trapping, manipulation, and detection of atoms with the single-seed laser system, exhibiting its applicability to atom interferometry and quantum sensing. The contrast of the signal is limited by residual magnetic fields, beam alignment, spontaneous emission, the atomic cloud temperature, and the finite size of the cloud within the Gaussian laser beam profile, none of which were fully optimized for this demonstration.

In conclusion, a wideband, agile, optical frequency generation scheme based on FBG technology was successfully demonstrated through the realization of a robust, alignment-free, single-seed, fiber laser system. The system was used to successfully laser cool and measure two-photon Raman transitions in ensembles of rubidium atoms. It exhibited exceptional modulation capabilities: the output frequency could be single-sideband modulated over a 30 GHz range with frequency switching in less than 40 ns; fast frequency and amplitude sweeping were enabled using DDS technology; and it had a 14.2 ± 0.3 ns amplitude rise time and 16.4 ± 0.2 ns fall time with an amplitude extinction ratio exceeding 80 dB. The output power was ∼0.5 W per output channel, limited by the output power of the EDFA and power handling capabilities of the AOM. An output power of ∼1 W per channel is expected by upgrading to 5 W EDFAs and AOMs.

Compared with previous single-seed laser systems for rubidium atom interferometry [11], the single-sideband modulation range was increased by a factor of 30 and the frequency switching time by a factor of 5000. This both increases the measurement bandwidth and can broaden the range of atom interferometry techniques available with single-seed laser systems.

Future versions could also enable filtering of the EOM harmonics by reducing the FBG reflection bandwidth and increasing the EOM frequency range such that the harmonics fall outside the FBG reflection bandwidth. Multiple EOMs and FBGs could also be used with the same seed laser to generate multiple independent outputs, enabling, for example, the generation of separate Raman I and II beams.

The system could be easily miniaturized to enable portable applications of atom interferometry and, in principle, the same agile frequency generation scheme could also be applied to other atomic species or quantum systems using similar components at different wavelengths. In the future, this could help facilitate a new generation of portable quantum devices.

Funding. Engineering and Physical Sciences Research Council (EP/T001046/1) as part of the UK National Quantum Technologies Programme.

Acknowledgment. We thank Farzad Hayati, Aisha Kaushik, Yu-Hung Lien, and Ben Stray for many useful discussions during the development of the laser system.

Disclosures. The authors declare no conflicts of interest.

Supplemental document. See Supplement 1 for supporting content.

REFERENCES

1. M. Kasevich and S. Chu, Phys. Rev. Lett. **67**, 181 (1991).
2. T. L. Gustavson, A. Landragin, and M. A. Kasevich, Class. Quantum Grav. **17**, 2385 (2000).
3. M. Kasevich and S. Chu, Appl. Phys. B **54**, 321 (1992).
4. J. M. McGuirk, G. T. Foster, J. B. Fixler, M. J. Snadden, and M. A. Kasevich, Phys. Rev. A **65**, 033608 (2002).
5. P. Asenbaum, C. Overstreet, M. Kim, J. Curti, and M. A. Kasevich, Phys. Rev. Lett. **125**, 191101 (2020).
6. C. Freier, M. Hauth, V. Schkolnik, B. Leykauf, M. Schilling, H. Wziontek, H.-G. Scherneck, J. Müller, and A. Peters, J. Phys. Conf. Ser. **723**, 012050 (2016).
7. A. Hinton, M. Perea-Ortiz, J. Winch, J. Briggs, S. Freer, D. Moustoukas, S. Powell-Gill, C. Squire, A. Lamb, C. Rammeloo, B. Stray, G. Voulazeris, L. Zhu, A. Kaushik, Y.-H. Lien, A. Niggebaum, A. Rodgers, A. Stabrawa, D. Boddice, S. R. Plant, G. W. Tuckwell, K. Bongs, N. Metje, and M. Holynski, Phil. Trans. R. Soc. A **375**, 20160238 (2017).
8. K. Bongs, M. Holynski, and Y. Singh, Nat. Phys. **11**, 615 (2015).
9. B. Cheng, P. Gillot, S. Merlet, and F. P. D. Santos, Phys. Rev. A **92**, 063617 (2015).
10. F. Theron, O. Carraz, G. Renon, N. Zahzam, Y. Bidel, M. Cadoret, and A. Bresson, Appl. Phys. B **118**, 1 (2015).
11. B. Battelier, B. Barrett, L. Fouché, L. Chichet, L. Antoni-Micollier, H. Porte, F. Napolitano, J. Lautier, A. Landragin, and P. Bouyer, Proc. SPIE **9900**, 990004 (2016).
12. J. Fang, J. Hu, X. Chen, H. Zhu, L. Zhou, J. Zhong, J. Wang, and M. Zhan, Opt. Express **26**, 1586 (2018).
13. D. M. S. Johnson, J. M. Hogan, S. W. Chiow, and M. A. Kasevich, Opt. Lett. **35**, 745 (2010).
14. O. Carraz, R. Charrière, M. Cadoret, N. Zahzam, Y. Bidel, and A. Bresson, Phys. Rev. A **86**, 033605 (2012).
15. L. Zhu, Y. Lien, A. Hinton, A. Niggebaum, C. Rammeloo, K. Bongs, and M. Holynski, Opt. Express **26**, 6542 (2018).
16. X. Li, L. Deng, X. Chen, M. Cheng, S. Fu, M. Tang, and D. Liu, Opt. Express **25**, 9333 (2017).
17. R. Boyd, *Nonlinear Optics* (Academic, 2008).
18. S. Dewra, V. Plaha, and A. Grover, Adv. Eng. Tec. Appl. **4**, 15 (2015).
19. TeraXion Inc., "TFN ultra narrowband tunable optical filter datasheet," https://teraxion.blob.core.windows.net/media/1355/teraxion-tfn-specsheet.pdf.
20. iXblue, "MPX and MPZ series datasheet," https://photonics.ixblue.com/sites/default/files/2020-02/MPX%2BMPZ%20SERIES.pdf.
21. D. J. McCarron, S. A. King, and S. L. Cornish, Meas. Sci. Technol. **19**, 105601 (2018).